Geophys. J. R. astr. Soc. (1978) **54**, 93–119

Shear deformation zones along major transform faults and subducting slabs

D. A. Yuen, L. Fleitout* and G. Schubert *Department of Earth and Space Sciences, University of California, Los Angeles, California, 90024, USA*

C. Froidevaux *Laboratoire de Physique des Solides, Université de Paris-Sud, Orsay, France, 91405*

Received 1977 November 15; in original form 1977 May 9

Summary. Narrow zones of intense shear deformation, i.e. viscous slip zones, are studied analytically with a one-dimensional time-dependent model of two half-spaces of identical or contrasting rheologies and ambient temperatures in relative motion. The rheologies of the half-spaces are strongly temperature-dependent and viscous heating maintains a thin zone of high temperature, low viscosity and large strain rate. The mathematical model is used to describe the structures of slip zones at ridge and plate-boundary transform faults, major continental strike–slip faults and at the top of subducting oceanic crust. No *a priori* assumption about slip-zone width or shear-stress magnitude is necessary; the thermal–mechanical structure of the slip zone evolves in time and all its characteristics are self-consistently determined. Slip-zone widths and shear stresses depend on the ambient temperatures, the relative velocity, the rheology and the length of time following the onset of relative motion; for reasonable geologic times, 0.1–10 Myr for example, slip zones are generally several kilometres wide and shear stresses are several hundred bars (tens of MPa). The region of intense shear in a viscous slip zone is an order of magnitude narrower than the width of the accompanying thermal anomaly. The maximum temperature generated by viscous dissipation in a slip zone depends only on the relative motion and the creep properties of the rocks; it is independent of slip-zone age and ambient temperature. Maximum temperatures associated with frictional heating are always less than those required for partial melting. The slip zone on a descending slab is influenced most strongly by the contrast in creep behaviour between the relatively soft oceanic crustal rocks and the hard, overlying mantle rocks; as a result, the slip zone is confined entirely within the oceanic crustal layer. Oceanic crustal rocks deform so readily that frictional heating in a slip zone on a descending slab cannot by itself lead to partial melting and thermal conduction from the hotter overriding mantle must play an essential role in heating the descending crust if

*Present address: Laboratoire de Physique des Solides, Université de Paris-Sud, Orsay, France, 91405.

melting is to occur therein. Because of the increase in the mantle temperature with depth, narrow slip zones in oceanic regions probably do not exist below depths of about 100 km; they may extend to greater depths beneath continents.

1 Introduction

The long-term relative motion along subduction zones and major transform faults is probably accommodated by viscous deformation at sufficiently high temperatures. Attendant frictional heating decreases the strongly temperature-dependent effective viscosity of mantle and crustal rocks, facilitating the deformation. As a result, such sites of mechanical decoupling, i.e. slip zones, are relatively narrow regions of high shear wherein heating by viscous dissipation leads to high temperature and low effective viscosity. Thermal–mechanical coupling, through viscous dissipation and the strongly temperature-dependent viscosity and the diffusion of heat, are the principal factors controlling slip-zone structure.

Turcotte & Oxburgh (1968) modelled the decoupling zone between plates in relative motion using a fluid dynamical theory which included frictional heating and a temperature-dependent viscosity. However, they had to make an *a priori* assumption about either the width of the shear zone or the magnitude of the shear stress to calculate the remaining characteristics of the slip zone. Bird, Toksöz & Sleep (1975) and Bird (1976, 1978) incorporated frictional heating into their models of continent–continent convergence by utilizing a one-dimensional theory of heating on a slip zone; they also had to make an essentially *a priori* specification of either slip-zone width or shear stress. However, for crustal and mantle rocks, the slip-zone width and the magnitude of the shear stress are coupled by frictional heating and the strong temperature-dependence of the viscosity; these quantities must be determined simultaneously and self-consistently. The ambiguity in shear-zone structure encountered in these papers is the result of the 'steady state' description attempted by the authors. Many other discussions of geodynamic processes at subduction zones (Jischke 1975) and transform faults (Lachenbruch & Thompson 1972; Aoki 1973; Lachenbruch & Sass 1973; Froidevaux 1973) have also been based on assumptions of slip-zone width or shear stress.

If the temporal development of a slip zone is considered, then there is no arbitrariness in any of its thermal or mechancial characteristics. In this paper we present a time-dependent, analytical model of the temperature, velocity, viscosity and shear stress in a slip zone; the model does not require any *a priori* assumptions about the width of the decoupling region or the magnitude of the shear stress. In addition, the model can describe slip zones between half-spaces with different ambient temperatures and contrasting rheologies. Such is the case for the slip zone on a descending slab between colder oceanic crust and hotter overriding mantle. The same may occur along an extended transform fault between oceanic and continental plates (e.g. the San Andreas) and along lengthy transform faults in continental interiors, where the geologic history is complex. In his studies of convergent continental margins, Bird (1978) stressed the importance of considering a crust with a weaker rheology than the mantle.

After presenting the mathematical theory and general results, we model slip zones on the descending lithosphere, on oceanic-ridge transform faults, on plate-boundary transform faults and on major continental strike–slip faults (Molnar & Tapponier 1975). Our models of slip zones on descending slabs clarify the role played by frictional heating in subduction-associated volcanism (McKenzie & Sclater 1968; Hasbe, Fujii & Uyeda 1970; Oxburgh & Turcotte 1970; Toksöz, Minear & Julian 1971; Turcotte & Schubert 1973). They also determine the frictional forces which resist plate motions at convergent boundaries (Richter 1977).

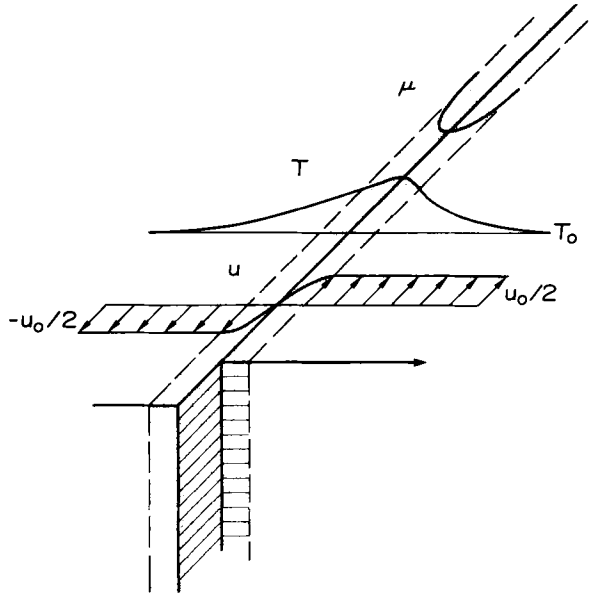

Figure 1. Sketch of the model involving shear between two identical half-spaces. The shaded area denotes the slip zone or region undergoing intense shear. T is the temperature, u is the velocity, and μ is the viscosity. T_0 is the ambient temperature, and the total relative velocity is u_0.

2 Theoretical models

2.1 IDENTICAL HALF-SPACES IN RELATIVE MOTION

Consider the development with time of the slip zone formed between two half-spaces of identical rheologies originally at rest with uniform temperature T_0. The half-spaces are in contact along the plane $y = 0$, and at time $t = 0$, they begin moving in opposite directions parallel to the interface with relative speed u_0. Fig. 1 is a sketch of the temperature $T(y)$, velocity $u(y)$, and viscosity $\mu(y)$ profiles in the slip zone at time t; a shear flow, confined mostly to the shaded region, accommodates the relative motion and a temperature anomaly has been established by frictional heating in the zone of shear. T tends to T_0 and the velocity u approaches $\pm u_0/2$ far from the interface. The temperature and the viscosity in the slip zone are symmetric about $y = 0$, while the velocity is antisymmetric. The shear zone thickens with time as frictional heat diffuses away from the interface.

Temperature and velocity are determined by the time-dependent equations

$$\rho \frac{\partial u}{\partial t} = \frac{\partial \tau}{\partial y} \tag{1}$$

$$\rho c_p \frac{\partial T}{\partial t} = k \frac{\partial^2 T}{\partial y^2} + \tau \frac{\partial u}{\partial y} \tag{2}$$

where ρ is the density, c_p is the specific heat at constant pressure, k is the thermal conductivity and τ is the shear stress. To these equations we must add a rheological law to determine τ.

Laboratory measurements of creep in crustal and mantle-type rocks indicate that strain rate is a non-linear function of stress; a dependence of the form $\partial u/\partial y \propto \tau^n$, with n generally

in the range 2 to 8, characterizes most of the laboratory data at stresses less than about a few kilobars (Stocker & Ashby 1973; Heard 1976). Strain rate is also dependent on the exponential of the inverse absolute temperature. This strong temperature dependence of the rheology is much more important in determining the character of flow in the mantle than is the non-linear dependence of strain rate on shear stress (Schubert, Froidevaux & Yuen 1976; Yuen & Schubert 1976). As long as n is not too large ($n \lesssim 9$), flow characteristics show only minor quantitative variations with n (Parmentier 1978).

Since the solution of equations (1) and (2) is facilitated by a linear or Newtonian relation between strain rate and shear stress and because we are mainly interested in the physical consequence of the temperature dependence of the rheology, we will approximate the non-linear creep of the mantle and crustal rocks with

$$\frac{\partial u}{\partial y} = \frac{2B}{T}\,\tau \exp\left(-Q/RT\right) \tag{3}$$

where R is the universal gas constant 1.987 cal/K mole (8.317 J/K mole), Q is the activation energy for creep and B is a material constant. The effective viscosity μ of material with the constitutive equation (3) is

$$\mu \equiv \tau/(\partial u/\partial y) = \frac{T}{2B} \exp\left(Q/RT\right). \tag{4}$$

We eliminate τ from equations (1) and (2) using the rheological law (3)

$$\rho \frac{\partial u}{\partial t} = \frac{\exp\left(Q/RT\right)}{2B}\left\{\frac{\partial u}{\partial y}\frac{\partial T}{\partial y}\left(1 - \frac{Q}{RT}\right) + T\frac{\partial^2 u}{\partial y^2}\right\}, \tag{5}$$

$$\rho c_p \frac{\partial T}{\partial t} = k\frac{\partial^2 T}{\partial y^2} + \frac{T}{2B}\exp\left(Q/RT\right)\left(\frac{\partial u}{\partial y}\right)^2. \tag{6}$$

The initial conditions for equations (5) and (6) are

$$T(y, 0) = T_0, u(y, 0) = H(y)\,u_0 - \tfrac{1}{2}u_0, \tag{7}$$

where $H(y)$ is the Heaviside function, and the boundary conditions for these equations are

$$\frac{\partial T}{\partial y}(0, t) = u(0, t) = 0, \tag{8}$$

$$T(\pm\infty, t) = T_0, u(\pm\infty, t) = \pm\frac{u_0}{2}. \tag{9}$$

Since $T(y, t)$ and $u(y, t)$ are even and odd functions of y respectively, it is sufficient to consider $y \geq 0$.

The coupled, non-linear, partial differential equations (5) and (6) with the initial and boundary conditions (7)–(9) can be reduced to a set of coupled, non-linear, ordinary differential equations by means of the similarity transformation $\eta = y/\sqrt{t}$

$$-\tfrac{1}{2}\rho\eta\frac{du}{d\eta} = \frac{\exp\left(Q/RT\right)}{2B}\left\{\frac{du}{d\eta}\frac{dT}{d\eta}\left(1 - \frac{Q}{RT}\right) + T\frac{d^2u}{d\eta^2}\right\}, \tag{10}$$

$$-\tfrac{1}{2}\rho c_p \eta\frac{dT}{d\eta} = k\frac{d^2T}{d\eta^2} + \frac{T}{2B}\exp\left(Q/RT\right)\left(\frac{du}{d\eta}\right)^2, \tag{11}$$

with the conditions

$$u(0) = \frac{dT}{d\eta}(0) = 0 \tag{12}$$

$$u(\infty) = u_0/2, \qquad T(\infty) = T_0. \tag{13}$$

The similarity form of solution depends on the consistency of initial conditions at $t = 0$ and boundary conditions at $y = \infty$ (since $\eta = y/\sqrt{t}$, both $t = 0$ and $y = \infty$ map into $\eta = \infty$). Thus, both conditions (7) and (9) are contained in conditions (13).

The equations and boundary conditions could be made dimensionless by introducing u_0, T_0 and $(k/\rho c_p)^{1/2}$ as scales for u, T and η, respectively. The system would then depend on only two dimensionless parameters, the Prandtl number Pr and the Brinkman number Br (Brinkman 1952)

$$\mathrm{Pr} = \mu(T_0)\, c_p/k, \tag{14}$$

$$\mathrm{Br} = \mu(T_0)\, u_0^2/kT_0. \tag{15}$$

Pr measures the relative importance of viscous and thermal diffusion and Br compares viscous dissipation and thermal conduction.

For the crust and mantle the Prandtl number is effectively infinite, i.e. thermal diffusion occurs on a very much longer timescale than does viscous diffusion and the inertial term in the equation of motion (the left side of equation (10)) can be neglected

$$T\frac{d^2u}{d\eta^2} + \left(1 - \frac{Q}{RT}\right)\frac{du}{d\eta}\frac{dT}{d\eta} = 0. \tag{16}$$

Frictional heat generated in the slip zone diffuses outward with time. At any particular time, temperature is a function of distance from the centre of the slip zone and, as a result, the strongly temperature-dependent viscosity μ varies considerably with y. But $\tau = \mu\partial u/\partial y$ must be independent of y if we neglect the inertial term in the equation of motion and $\partial u/\partial y$ must adjust to accommodate the spatial dependence of μ. As $T(y)$ and hence $\mu(y)$ change with time, $\partial u/\partial y$ also varies with t. Thus the temporal evolution of the flow profile in the slip zone occurs on the thermal-diffusion timescale. The Brinkman number alone governs the spatial and temporal development of the slip zone.

Shear heating in a medium whose viscosity is exponentially dependent on T or T^{-1} is a phenomenon encountered in many industrial situations (Gavis & Laurence 1968; Turian 1969). An example is die entry in polymer melt processing, where Br is 10^2–10^3 and Pr is 10–10^2. Whereas the evolution of the slip zone in the Earth takes place on a thermal-diffusion time, these more comparable values of Br and Pr lead to interesting coupling in which both viscous and thermal diffusion govern the time development of the shear flow.

The equations (11) and (16) and boundary conditions (12) and (13) constitute a two-point boundary value problem for u and T. We have solved the system using a Newton–Raphson iteration procedure; values of $T(0)$ and $du/d\eta(0)$ are adjusted in this iterative scheme until conditions (13) are satisfied at some large value of η, η_{max}. The solutions are acceptable only when they are insensitive to changes in η_{max}.

2.2 HALF-SPACES OF CONTRASTING TEMPERATURE AND RHEOLOGY IN RELATIVE MOTION

We next develop the one-dimensional, time-dependent model of the slip zone between two half-spaces with different rheologies and ambient temperatures. We consider all of the de-

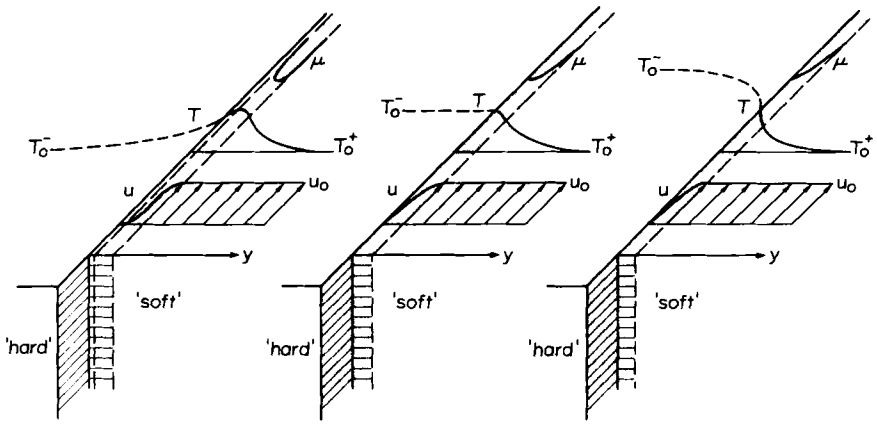

Figure 2. Model of shear deformation between two half-spaces with vastly different rheologies. 'Hard' and 'soft' describe the relative ductility of the two materials. The slip zones are indicated by the shaded areas. T_0^- and T_0^+ are the ambient temperatures of the 'hard' and 'soft' half-spaces respectively. Three different situations are shown – no heat transfer at the interface, or heat flow into or out of the soft medium. The total relative velocity is u_0 and all the deformation takes place in the soft half-space.

coupling to occur within the 'soft' half-space ($y \geqslant 0$) of crustal material, as shown by the shaded regions in Fig. 2; the 'hard' half-space can be considered to be made of mantle material. We allow the half-spaces of contrasting rheologies to have different initial temperatues, T_0^- and T_0^+ for $y < 0$ and $y > 0$, respectively. The figure shows qualitative velocity, temperature and viscosity profiles at some time t after relative motion begins for three different initial thermal states. On the left $T_0^- = T_0^+$; note that the shear occurs at a small distance from the interface $y = 0$. In the middle, T_0^- and T_0^+ are such that there is no heat transfer between the half-spaces and T is constant in the hard material. Deformation begins immediately at the interface. On the right $T_0^- > T_0^+$ and heat flows from the hard to the soft half-space. Again the slip zone is adjacent to the interface.

The equations of motion and temperature in the soft half-space are equation (5), with the left side equal to zero and equation (6). In the harder material only the temperature equation (6) without the frictional-heating term needs to be considered. The initial conditions are

$$T(y, 0) = T_0^+, \text{ for } y > 0, \qquad T(y, 0) = T_0^- \text{ for } y < 0, \tag{17}$$

$$u(y, 0) = H(y)u_0. \tag{18}$$

Far from the interface we require

$$T(\infty, t) = T_0^+, \qquad T(-\infty, t) = T_0^-, \qquad u(\infty, t) = u_0. \tag{19}$$

At the interface, the velocity is zero since the hard medium does not deform and it is assumed stationary

$$u(0, t) = 0. \tag{20}$$

The temperature and heat flux are continuous at $y = 0$

$$T(0-, t) = T(0+, t), \tag{21}$$

$$k_- \frac{\partial T}{\partial y}(0-, t) = k_+ \frac{\partial T}{\partial y}(0+, t), \tag{22}$$

where k_- and k_+ are the thermal conductivities for $y < 0$ and $y > 0$, respectively.

The equations and initial, boundary and interface conditions are consistent with a solution in terms of the similarity variable η. The equations for T and u in the soft half-space in terms of η are equations (11) and (16). In the hard material $y < 0, u \equiv 0$ and T satisfies (11) without the viscous dissipation term. The initial, boundary and interface conditions, in terms of η are

$$T(-\infty) = T_0^-, \qquad T(\infty) = T_0^+, \qquad u(\infty) = u_0, \tag{23}$$

$$T(0-) = T(0+), k_- \frac{dT}{d\eta}(0-) = k_+ \frac{dT}{d\eta}(0+), u(0) = 0. \tag{24}$$

In the half-space of hard material, $\eta < 0$, the temperature is simply

$$T(\eta) = T(0-) + \frac{dT}{d\eta}(0-)\left(\frac{\pi k_-}{\rho c_p}\right)^{1/2} \operatorname{erf}\left(\frac{\eta}{2}\left(\frac{\rho c_p}{k_-}\right)^{1/2}\right). \tag{25}$$

The temperature T_0^- must be obtained as $\eta \to -\infty$

$$T_0^- = T(0-) - \frac{dT}{d\eta}(0-)\left(\frac{\pi k_-}{\rho c_p}\right)^{1/2}. \tag{26}$$

From continuity of temperature and heat flux at $\eta = 0$ (equation (24)), equation (26) may be rewritten

$$T(0+) = T_0^- + \frac{k_+}{k_-}\frac{dT}{d\eta}(0+)\left(\frac{\pi k_-}{\rho c_p}\right)^{1/2}. \tag{27}$$

Temperature and velocity in the deformable half-space $y > 0$ are solutions of equations (11) and (16) subject to the conditions $u(0) = 0$, $u(\infty) = u_0$, $T(\infty) = T_0^+$ and equation (27). The only difference between this problem and the one already solved is the boundary condition (27); we previously had $dT/d\eta(0+) = 0$ and we now have a condition relating to $T(0+)$ and $dT/d\eta(0+)$. Thus we can solve for T and u in the deformable region $\eta > 0$ exactly as before.

3 Thermodynamic and rheological parameter values for crustal and mantle rocks

The thermodynamic properties are relatively straightforward; for the densities of mantle and crustal rocks we choose 3.3 and 3.0 g/cm^3, for the thermal conductivities of mantle and crust we use 0.008 cal/cm s K (0.033 J/cm s K) and 0.006 cal/cm s K (0.025 J/cm s K) and for the specific heat at constant pressure we take 0.27 cal/g K (1.13 J/g K) in both the mantle and crust.

The creep of olivine, for which $n = 3$ (Kohlstedt & Goetze 1976; Kohlstedt, Goetze & Durham 1976), likely controls deformation in the Earth's upper mantle. However, because the mineralogies and compositions of oceanic and continental crusts are complex and heterogeneous, it is not clear which mineral, if any single one, controls crustal creep. Thus we employ the rheologies of dry and wet olivine to model the viscous deformation of the mantle and the rheologies of Maryland diabase, wet quartzite and limestone to model the viscous creep of crustal rocks. The laboratory-determined creep laws for these rocks are listed in Table 1. We have modified the experimental flow laws given in the references to incorporate a $1/T$ dependence suggested by theoretical models of creep (Herring 1950). The empirical pre-exponential coefficient was equated to B/T at the maximum temperature generated in a slip zone between identical half-spaces with $u_0 = 10$ cm/yr. Of all the rocks listed in Table 1, dry olivine is the most difficult to deform. The crustal materials are all

Table 1. Rheological parameters [du/dy has units (/s), τ has units (dyne/cm^2) or (0.1 Pa), RT has units (cal/mole) or (4.185 J/mole) T is in (K)].

	Experimental creep law	Q(kcal/mole) or (4.185 kJ/mole)	B(K s cm/g)
Dry olivine	$\frac{du}{dy} = \frac{1.3 \times 10^{-12}}{T} \tau^3 \exp\left(\frac{-125\,000}{RT}\right)$ Kohlstedt & Goetze (1974) Schubert *et al.* (1976)	129	5.2×10^5
Wet olivine	$\frac{du}{dy} = \frac{1.1 \times 10^{-13}}{T} \tau^3 \exp\left(\frac{-95\,000}{RT}\right)$ Post (1977) Schubert *et al.* (1976)	99	4.4×10^3
Maryland diabase	$\frac{du}{dy} = \frac{1.0 \times 10^{-15}}{T} \tau^3 \exp\left(\frac{-85\,000}{RT}\right)$ Goetze & Brace (1972) Tapponier & Francheteau (1977)	89	1.8×10^2
Wet quartzite	$\frac{du}{dy} = \frac{4.7 \times 10^{-17}}{T} \tau^{2.6} \exp\left(\frac{-55\,000}{RT}\right)$ Parrish, Krivz & Carter (1976)	59	2.6×10^{-3}
Limestone	$\frac{du}{dy} = \frac{2.2 \times 10^{-8}}{T} \tau^{2.05} \exp\left(\frac{-50\,400}{RT}\right)$ Schmid (1976)	54.4	1.8×10

weaker than wet or dry olivine. All the rocks of Table 1 deform non-linearly, with n between 2 and 3. They span the range of activation energies between about 50 and 125 kcal/mole (0.2 and 0.5 MJ/mole).

The similarity solution requires linear approximations to the non-linear, experimental creep laws. These approximations are made by adjusting Q and B to match the real rheological law under conditions of stress and temperature in the slip zone.

We use the measured value of activation energy for Q (the Q values given in Table 1 include an additional 4 kcal/mole (16.7 kJ/mole) to account for the small effect of pressure on the creep of rocks at depths less than about 100 km). The value of B was determined by equating the strain rate computed from equation (3) to that computed from the empirical equation at a temperature very nearly equal to the maximum temperature in a slip zone between identical half-spaces with a differential velocity $u_0 = 10$ cm/yr. Some iteration between the calculation of slip-zone temperature and the choice of B is required. We match the strain rates at stresses which are representative of those which occur after a few million years of slip when the relative motion is 10 cm/yr (600 bars (60 MPa) for crustal rocks and 900 bars (90 MPa) for wet and dry olivine). The values of B determined in this way are listed in Table 1. The empirical stress–strain rate equations for all the materials listed in Table 1 are plotted in Fig. 3 together with the linear approximations.

4 Temperature, velocity, viscosity and shear stress in the slip zone between identical half-spaces

In this section we discuss how rheology influences the structure of a slip zone between identical half-spaces with $T_0 = 400$ K, moving relative to each other at 10 cm/yr, 2 M yr after the onset of shear.

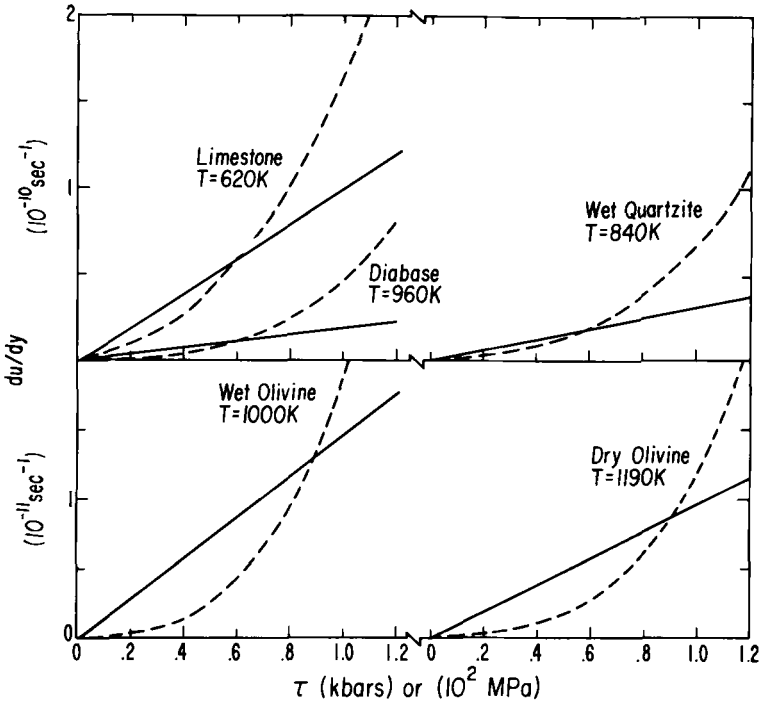

Figure 3. Comparison between the laboratory flow laws of crustal and mantle rocks and the linear approximations. The listed temperatures are approximately the maximum temperatures produced in a slip zone between identical half-spaces with $u_0 = 10$ cm/yr. These are the temperatures at which values of the rheological parameter B were determined, as described in the text. The dashed curves are the empirical flow laws, and the solid lines represent the linear approximations. The linear approximations and the non-linear creep laws are matched at 600 bar (60 MPa) for crustal material and at 900 bar (90 MPa) for olivine.

4.1 TEMPERATURE AND VELOCITY

Fig. 4 shows temperature and velocity profiles for all five crustal and mantle rheologies. Temperature in the slip zone is strongly influenced by rheology; the slip zone is cooler the more readily deformable the material. The maximum temperature at the centre of the slip zone T_{max} depends essentially only on u_0 and the rheological parameters. T_{max} is independent of time because of the similarity form of the solution and, as the following shows, it is also essentially independent of T_0.

A simple formula for T_{max} can be derived from the steady-state equations. With $\partial/\partial t = 0$ and τ = constant, equation (2) integrates to

$$\frac{dT}{dy} = \frac{-\tau u}{k}. \tag{28}$$

If equation (28) is used to eliminate u from equation (6), the resulting equation can be integrated to yield

$$\left(\frac{dT}{dy}\right)^2 = \frac{4B\tau^2}{k}\left\{E_1\left(\frac{Q}{RT_{max}}\right) - E_1\left(\frac{Q}{RT}\right)\right\}, \tag{29}$$

where E_1 is the exponential integral (Abramowitz & Stegun 1965). Both τ and dT/dy can be eliminated between equations (28) and (29) to give

$$u^2 = 4kB\left\{E_1\left(\frac{Q}{RT_{max}}\right) - E_1\left(\frac{Q}{RT}\right)\right\}. \tag{30}$$

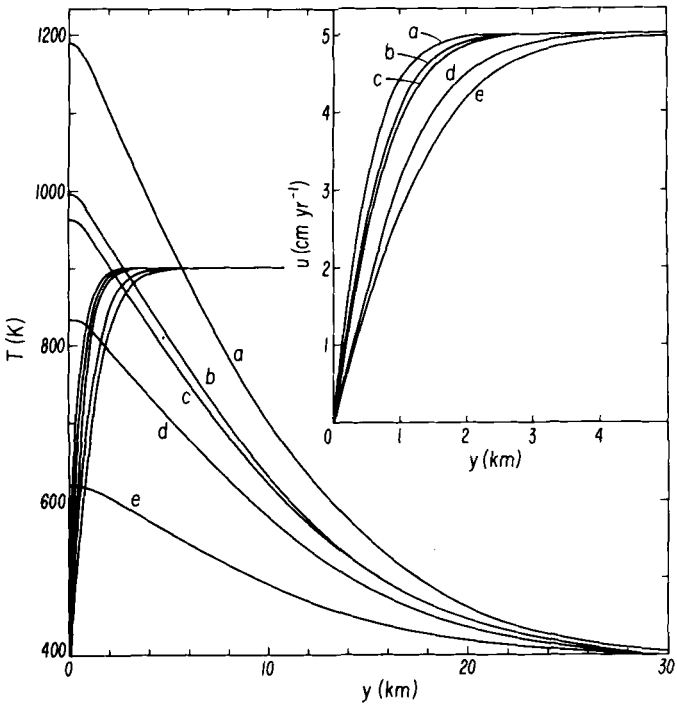

Figure 4. Temperature and velocity profiles for slip zone between identical crustal and mantle half-spaces at $t = 2$ Myr; (a) dry olivine (b) wet olivine (c) diabase (d) wet quartzite (e) limestone. $u_0 = 10$ cm/yr, $T_0^- = T_0^+ = T_0 = 400$ K.

With $u(\infty) = u_0/2$ and $T(\infty) = T_0$, equation (30) gives an implicit formula for $T_{\max}$

$$u_0^2 = 16kB\left\{E_1\left(\frac{Q}{RT_{\max}}\right) - E_1\left(\frac{Q}{RT_0}\right)\right\}. \tag{31}$$

For crustal and mantle temperatures and creep activation energies, Q/RT_0 is larger than $Q/RT_{\max}$, which in turn is very much larger than unity. The exponential integral then has a simple asymptotic form and equation (31) simplifies to

$$u_0^2 \approx \frac{16kBRT_{\max}}{Q} \exp\left(\frac{-Q}{RT_{\max}}\right). \tag{32}$$

A similar result, based on a graphical integration, was obtained by Turcotte & Oxburgh (1968). T_0 does not significantly influence $T_{\max}$ provided

$$E_1\left(\frac{Q}{RT_0}\right) \ll E_1\left(\frac{Q}{RT_{\max}}\right).$$

Equation (32) and the exact time-dependent similarity solution give the same values of $T_{\max}$, namely, 1190, 999, 963, 834 and 619 K for dry olivine, wet olivine, diabase, wet quartzite and limestone respectively. The approximation is successful because most of the shear occurs where T is close to $T_{\max}$. Since $T_{\max}$ is independent of time, the temperature in most of the shear region is also approximately independent of time.

The extent of the thermal anomaly can be measured by the thermal boundary-layer thickness δ_T, i.e. the distance from the centre of the slip zone to the location where $(T - T_0)$

has decayed to 10 per cent of $(T_{max} - T_0)$. δ_T is about 19 km for all the temperature profiles in Fig. 4. Thermal boundary-layer thickness is insensitive to the rheological parameters. For all the solutions of Fig. 4 the velocity has its asymptotic value within 3 km of the centre of the slip zone. If a mechanical boundary-layer thickness δ_m is defined as the distance from $y = 0$ to the location where the velocity increases to 90 per cent of its asymptotic value, $u_0/2$, then δ_m has the values 1, 1.25, 1.4, 2.0, 2.4 km for dry olivine, wet olivine, diabase, wet quartzite and limestone respectively. The thermal anomaly extends about an order of magnitude further from the centre of the slip zone than does the region of shear. These shear regions are much narrower than previous estimates (Turcotte & Oxburgh 1968; Jischke 1975). Most of the shear occurs in that part of the slip zone where T is within about 25 K of T_{max}.

4.2 VISCOSITY

The viscosity profiles corresponding to the solutions in Fig. 4 are shown in Fig. 5. The curves are solid in that region of the slip zone where $y < \delta_m$. The minimum viscosity occurs at $y = 0$ where T is a maximum. These minimum viscosity values are relatively insensitive to rheology and lie between about 2 and 6×10^{20} poise (2 and 6×10^{19} Pa s). The low viscosities are required to sustain the high strain rates of $0(10^{-12}\,s)$ which are at least an order of magnitude larger than those typically associated with global plate tectonics. Throughout most of the shear zone, the viscosity remains less than about 3×10^{21} poise (3×10^{20} Pa s), independent of rheology. The thermal-feedback mechanism maintains a relatively constant value of viscosity in the region of shear by adjusting T_{max} according to the particular rheological parameters. Outside the region where most of the shear occurs the viscosity rises rapidly by many orders of magnitude; the viscosity changes by 4–5 orders of magnitude in a distance of only several kilometres.

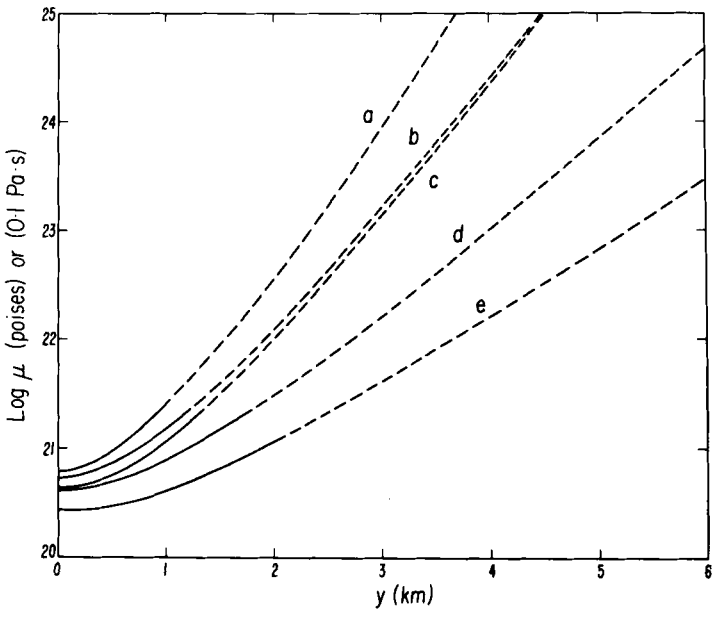

Figure 5. Viscosity profiles for the solutions (a)–(e) of Fig. 4. The solid portions of the curves give the viscosities in the slip zones, $y \leqslant \delta_m$.

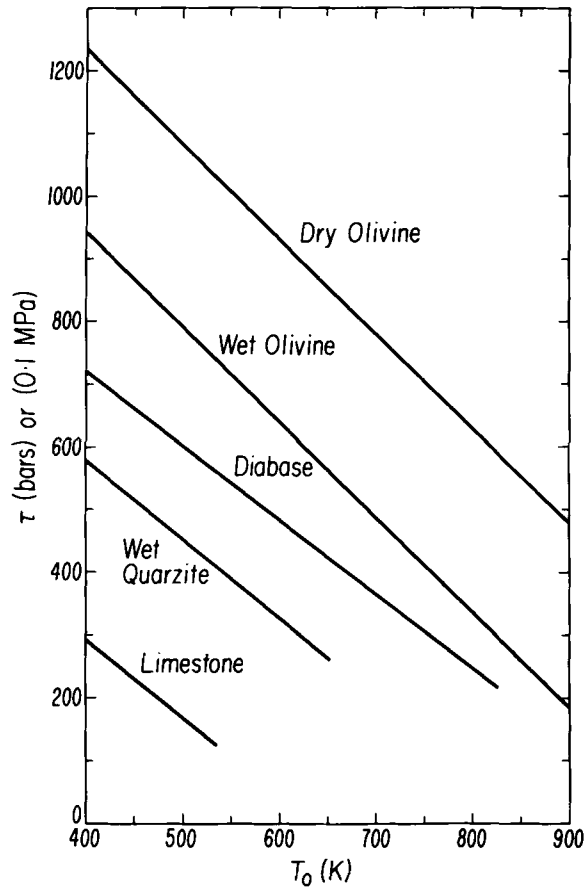

Figure 6. Shear stress τ in the slip zone between identical half-spaces in relative motion versus ambient temperature T_0 for various mantle and crustal rheologies. $u_0 = 10$ cm/yr, $t = 2$ M yr.

4.3 SHEAR STRESS

The shear stresses corresponding to the solutions of Figs 4 and 5 are 1230, 942, 720, 578 and 293 bars (bar = 0.1 MPa) for dry olivine, wet olivine, diabase, wet quartzite and limestone respectively. Fig. 6 shows how τ changes with rheology and with T_0. τ varies from hundreds of bars (10 MPa) for the weak crustal rocks to more than a kilobar (100 MPa) for dry olivine. Recall that τ is independent of y and varies as $t^{-1/2}$ (the stresses in Fig. 6 are at $t = 2$ M yr). The results show that τ decreases almost linearly with increasing T_0.

5 Dependence of slip-zone structure on T_0 and u_0

We have chosen the wet olivine rheology to illustrate how variations in T_0 and u_0 influence slip-zone structure. Fig. 7 shows temperature and velocity profiles for $u_0 = 10$ cm/yr, $T_0 = 400$, 600 and 800 K and $t = 0.5$, 2 and 8 M yr. The widening of the thermal anomaly and the region of shear with $t^{1/2}$ are readily seen. T_{max} is 999 K, independent of t and T_0. δ_T is insensitive to changes in ambient temperature. However, the region of shear is observed to broaden with increasing T_0. At $t = 2$ M yr, δ_m is about 1.4, 2.0 and 3.0 km for $T_0 = 400$, 600 and 800 K respectively.

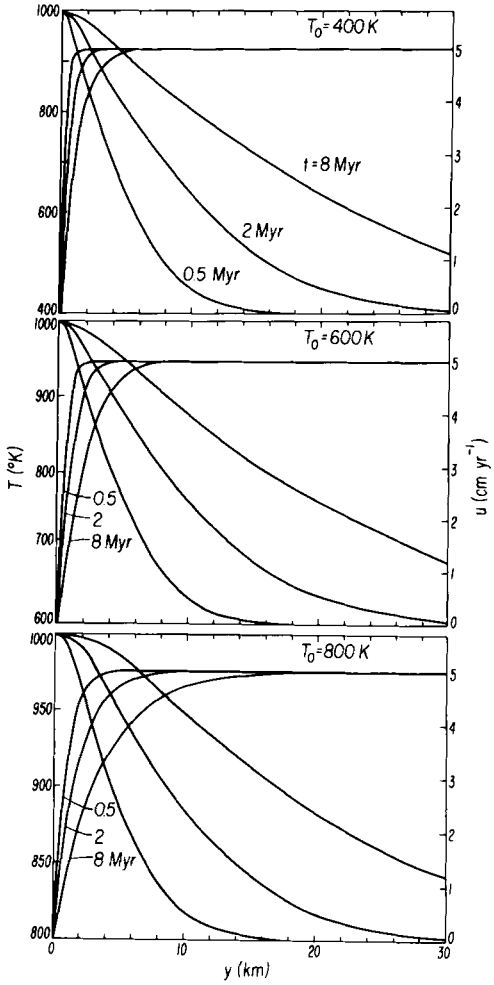

Figure 7. Temperature and velocity fields between identical half-spaces in relative motion for three ambient temperatures at t = 0.5, 2 and 8 M yr. The rheology is wet olivine and u_0 = 10 cm/yr.

Not only is δ_T insensitive to changes in T_0, but so is $\Theta = (T - T_0)/(T_{max} - T_0)$. From equation (4), we can write μ in terms of Θ as

$$\mu = \left(\frac{T_0(1-\Theta) + T_{max}\Theta}{2B}\right) \exp\left(\frac{Q/R}{T_0(1-\Theta) + T_{max}\Theta}\right). \tag{33}$$

Since Θ and T_{max} are independent of T_0, equation (33) shows that at a given y, μ decreases with increasing T_0. This accounts for the broadening of the slip zone with increasing T_0. The viscosity profiles at t = 2 M yr are shown in Fig. 8 for different T_0. The solid parts of the profiles again indicate the width of the region of shear. Since T_{max} is a function only of u_0 for a given rheology, the same is true of the minimum viscosity.

When the ambient temperature is larger than about 860 K, T_0 is sufficiently close to T_{max} (999 K) that there is relatively little viscosity variation with y. In this case, $\partial u/\partial y$ is no longer sufficiently small at the maximum limit of integration, η_{max}, compared to its value in the slip zone (10^{-15} s compared to 10^{-12} s), that the solution is independent of the particular

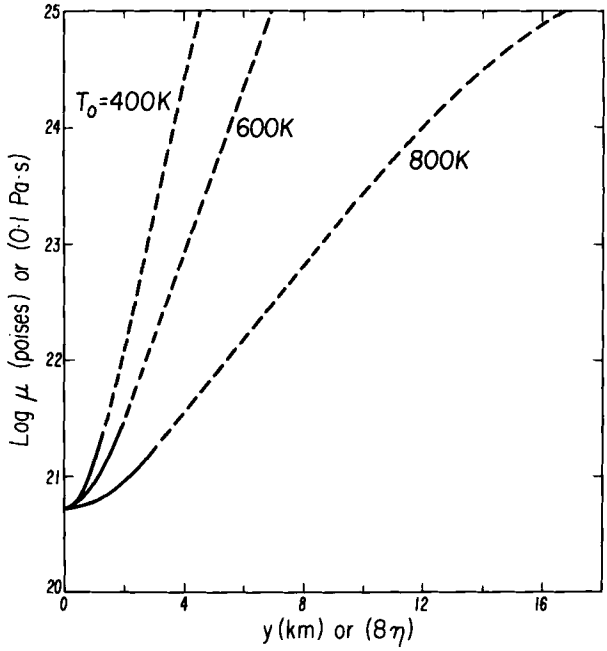

Figure 8. Viscosity structure between identical wet olivine half-spaces in relative motion for different values of the ambient temperature T_0. The solid portions of the curves lie within the slip zone, $y \leqslant \delta_m$. u_0 = 10 cm/yr, t = 2 M yr.

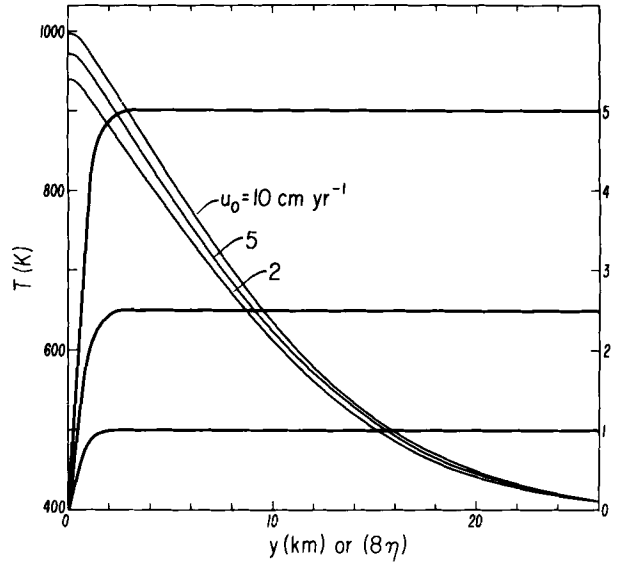

Figure 9. The effects of u_0 on the temperature and velocity structures between identical wet olivine half-spaces with T_0 = 400 K at t = 2 M yr.

value of η_{max} (η_{max} was 15 $(k/\rho c_p)^{1/2}$ for the solutions reported in this paper). At ambient temperatures approaching T_{max}, the notion of a narrow slip zone describable by a one-dimensional model probably is no longer a useful concept because of the relatively small viscosity variations which occur in the region of shear.

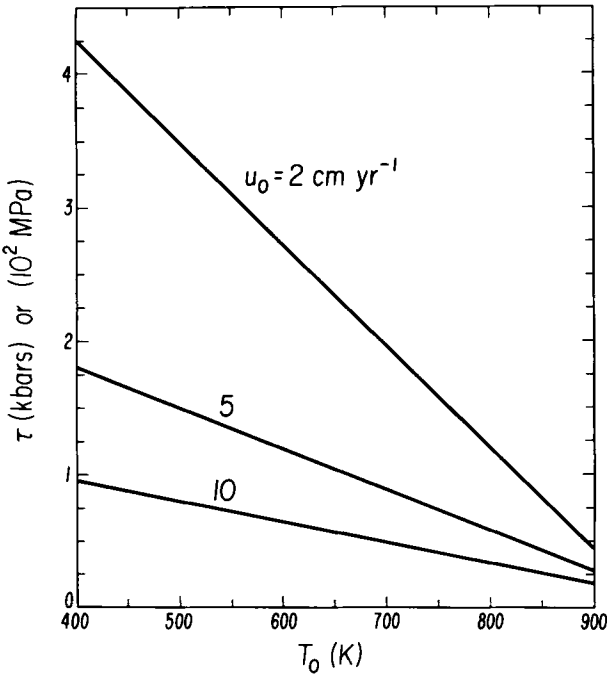

Figure 10. The dependence of shear stress τ on ambient temperature T_0 for different relative velocities u_0. Wet olivine rheology and $t = 2$ M yr.

The effects on T and u of varying the relative velocity u_0 are shown in Fig. 9 for wet olivine with $T_0 = 400$ K at $t = 2$ M yr. Values of u_0 equal to 2, 5 and 10 cm/yr are considered. The amount of shear heating increases with u_0; T_{max} is 939, 972 and 999 K, for $u_0 = 2$, 5 and 10 cm/yr respectively. The variation of T_{max} with u_0 is accurately represented by equation (32). δ_T and δ_m are insensitive to changes in u_0.

The dependence of shear stress on u_0 can be seen in Fig. 10 where τ is shown as a function of T_0 for $u_0 = 2$, 5 and 10 cm/yr ($t = 2$ M yr and the material is wet olivine). τ is approximately inversely proportional to u_0 since viscous dissipation is the sole source of heating in the slip zone. Actual crustal and mantle rocks could not maintain the large stresses implied by our viscous model, for small relative velocities, without fracturing. The implication is that slip zones exist only for sufficiently rapid relative motion.

5 Temperature, velocity, viscosity and shear stress in the slip zone between hard and soft materials

5.1 TEMPERATURE AND VELOCITY

We have calculated T and u profiles for a slip zone formed by the relative motion of a half-space with a soft crustal rheology and a half-space with a hard mantle rheology. In all these calculations, u_0 was 10 cm/yr and T_0^+ was 400 K. The results are shown in Fig. 11 for all three crustal rheologies at a time of 2 M yr.

The solutions depend on T_0^-, the ambient temperature in the hard material far from the slip zone. Depending on the relative values of T_0^- and T_0^+, a variety of solutions are obtained; the heat flux can be zero at the interface, or it can be non-zero and directed either into the mantle or crust. We have thus considered three situations to represent these possibilities.

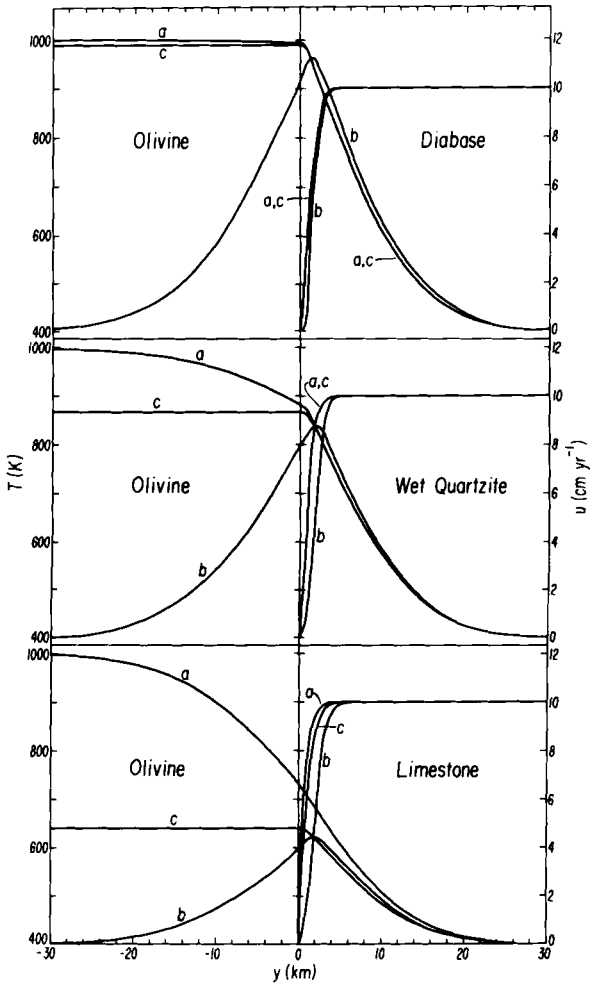

Figure 11. Temperature and velocity profiles between olivine and crustal half-spaces in relative motion. In all cases T_0^+ is 400 K and u_0 = 10 cm/yr. (a) T_0^- = 1000 K, (b) T_0^- = 400 K and (c) no heat is transferred between the two half-spaces. t = 2 M yr.

In one case (a) T_0^- = 1000 K and heat flows from the mantle to the crustal material. In another case (b) T_0^- = 400 K and the direction of heat flow is reversed. Finally, in the third case (c) T_0^- is adjusted to give a zero heat flux at the interface.

For T_0^- = 1000 K (a) heat flows into the crustal half-spaces and deformation in the soft crusts occurs in narrow zones, less than 2.5 km wide, adjacent to the interface. When T_0^- = 400 K (b) deformation occurs in zones less than 3 km wide at a distance of about 1.5 km from the interface. There is a net heat flow into the hard material and the maximum temperatures in the crust occur away from the interface ($\approx$1.5 km). When T_0^- = 638, 867 and 992 K (c) for limestone, wet quartzite and diabase respectively, there is no heat flow into the undeformable half-space. The maximum temperatures in the weak crust occur at the interface and the temperatures in the hard mantle are uniform. The interface temperatures for zero heat flux at the interface can be obtained from equation (32) if u_0 in that equation is 20 cm/yr. The narrow shear zones are immediately adjacent to the interface.

For the soft crustal materials shear profiles are very similar. The weak layer begins to deform right at the interface unless the hard material is relatively cold. For both wet quartzite and diabase the thermal structures in cases (a) and (c) are nearly the same, especially in the crust. For limestone, the thermal profiles in these cases are more distinct. When the hard material is cold far from the interface (b), thermal profiles are especially distinct in the hard mantle. When T_0^- varies between 400 and 1000 K, the interface temperature changes by only about 100 K, for all the crustal rheologies in Fig. 11. In all the cases (a), (b) and (c) the crustal temperatures are lower, the weaker the material. Limestone is so soft that the temperatures in the crust within 5 km of the interface are about 200 K lower than temperatures in either wet quartzite or diabase.

5.2 VISCOSITY

Our model of the slip zone between half-spaces of contrasting rheologies is based on the assumption that the viscosity of the hard material is at least several orders of magnitude larger than the viscosity in the crustal slip zone. To verify this we have calculated the viscosity profiles corresponding to the three solutions presented in Fig. 11 for diabase slipping against dry olivine. The results are shown in Fig. 12; the profiles labelled (a), (b) and (c) are associated with similarly designated curves in Fig. 11. The dashed positions of the profiles denote regions where there is virtually no shear.

For cases (a) and (c) the viscosity in the olivine half-space is more than five orders of magnitude higher than the minimum viscosity in the crustal slip zone; the viscosity in the crustal slip zone increases by less than an order of magnitude. The viscosity jump is even

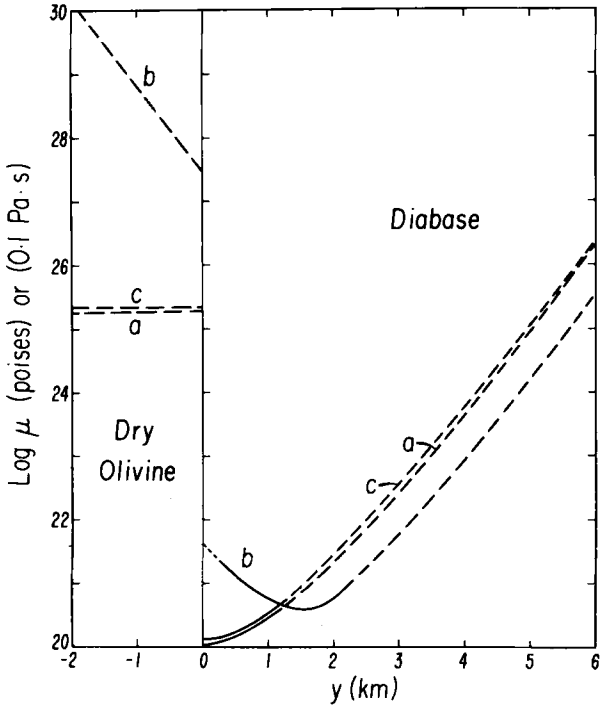

Figure 12. Viscosity profiles between diabase and dry olivine half-spaces in relative motion. Curves labelled (a), (b) and (c) correspond to the T and u profiles shown in Fig. 11. Where the curves are solid, the shear is large; where the curves are dashed, there is relatively no deformation.

Table 2. Shear stress (bar) or (0.1 MPa) in slip zones between hard mantle and soft crustal half-spaces in relative motion (u_0 = 10 cm/yr, t = 2 M yr).

	Limestone	Wet quartzite	Diabase
$T_0^- = T_0^+ = 400$ K	314	624	806
$(dT/dy)_{y=0} = 0$, $T_0^+ = 400$ K	160	312	386
$T_0^- = 1000$ K, $T_0^+ = 400$ K	1.7	225	382

larger in case (b). The viscosity contrasts between wet quartzite and dry olivine and between limestone and dry olivine, for the solutions of Fig. 11 are even more dramatic. Thus we are justified in adopting the assumption that essentially all deformation occurs within the soft crust. However, if T_0^- is larger than about 1100 K, for dry olivine, the viscosity of the half-space $y < 0$ is not large enough to ignore deformation within it; in fact, the concept of a slip zone breaks down.

5.3 SHEAR STRESS

The shear stresses for the solutions discussed in Figs 11 and 12 are listed in Table 2. They are all several hundred bars (tens of MPa) except in the case of a limestone half-space sliding against a relatively hot, olivine half-space, in which case τ is a few bars (tenths of MPa). The rheological parameter B, which was determined by matching strain rates from an approximate linear flow law and the empirical flow law at 600 bar (60 MPa), should be re-adjusted in these cases of low τ.

Values of τ given in Table 2 for $T_0^+ = T_0^- = 400$ K are larger than the shear stresses associated with the slip zone between two half-spaces of the same rheology (see Fig. 6). The larger τ for contrasting rheologies is due to the leakage of frictional heat into the undeformable material.

5.4 ASSESSMENT OF FRICTIONAL HEATING

When the ambient temperatures are the same the entire thermal anomaly is due to frictional heating. The top of Fig. 13 illustrates this for wet quartzite with $u_0 = 10$ cm/yr, $t = 2$ M yr and $T_0^+ = T_0^- = 400$ K. The shaded area represents that part of the temperature anomaly which is directly attributable to shear heating. The middle of Fig. 13 shows the temperature profile for $T_0^- = 867$ K which corresponds to zero heat flux at the interface (the other parameter values are unchanged). This is the curve at the top of the shaded region. The bottom of the shaded region is the temperature profile due to thermal diffusion alone 2 M yr after half-spaces with $T_0^- = 867$ and $T_0^+ = 400$ K come into contact. The shaded area is thus a measure of the excess temperature due to viscous dissipation. Frictional heating in the crust offsets the cooling of the hard half-space and maintains its temperature constant. The bottom of Fig. 13 shows a similar situation with $T_0^- = 1000$ and $T_0^+ = 400$ K.

6 Slip zones along transform faults

6.1 RIDGE TRANSFORM FAULTS

Earthquakes at ridge transform faults occur no deeper than 10 km according to seismic studies using sonobuoys (Reid & McDonald 1973; Reichle 1975). Below this depth, viscous

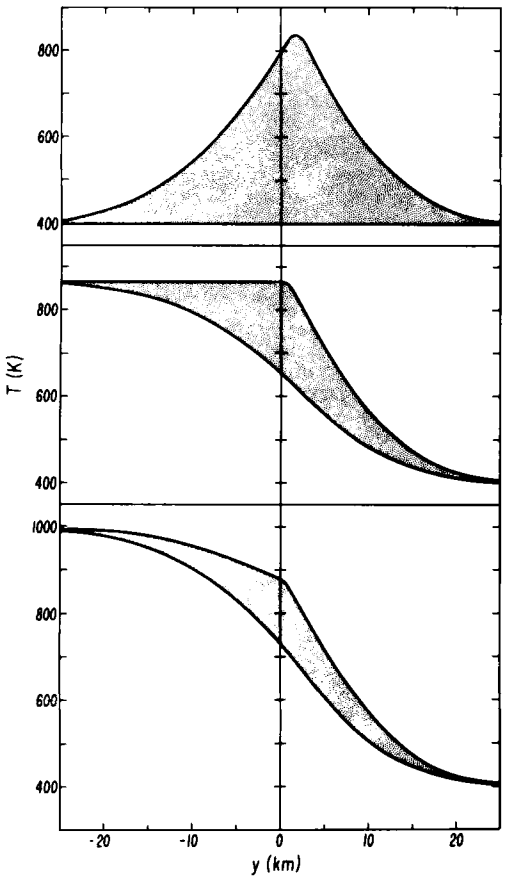

Figure 13. Excess temperatures due to frictional heating in the slip zone within a wet quartzite half-space sliding past an olivine half-space at $u_0 = 10$ cm/yr, $t = 2$ Myr, $T_0^+ = 400$ K. Top: $T_0^- = 400$ K. Middle: no heat flux at interface. Bottom: $T_0^- = 1000$ K. The curve forming the upper boundary of the shaded area is the actual temperature profile. The curve forming the lower border is the T profile resulting from pure thermal diffusion after the half-spaces are placed in contact at $t = 0$ with no relative motion. The shaded area is thus a measure of the excess temperatures caused by frictional heating.

slip is likely to occur (Aoki 1973; Froidevaux 1973; Oldenburg & Brune 1975). Thus we apply our model of viscous slip between identical half-spaces to the Romanche fracture zone in the Atlantic Ocean, the Eltanin fracture zone in the Pacific Ocean and the Amsterdam fracture zone in the Indian Ocean. Table 3 gives T_{max}, τ, δ_m and δ_T at the midpoints of these long ridge transform faults where end effects are probably unimportant. The relative motions are from Minster *et al.* (1974) and lithosphere thicknesses are estimates from model calculations of Yuen, Tovish & Schubert (1978) and from a number of our unpublished results. Since the oceanic lithosphere below 10 km depth is composed mainly of peridotite, we used wet and dry olivine rheologies to describe the creep behaviour. The structure of the slip zone was investigated at depths of 10, 20 and 30 km; T_0 at these depths was estimated from $T(^\circ\text{C}) = (1200^\circ\text{C})\,\text{erf}\,(\tfrac{1}{2}\,\text{depth}\,(\rho c_p/k\,\text{age})^{1/2})$.

Since T_{max} depends only on u_0 and rheology, it is independent of depth on the fault; the u_0 dependence is so weak that T_{max} is only about 50 K larger for the faults in the faster spreading oceans. T_{max} is also well below the melting temperature of either wet or dry olivine at these shallow depths. τ decreases with depth on the fault because of the increase

Table 3. Application of the identical half-space model to ridge transform faults. (T_0 and T_{max} are in (K), τ is in bar (0.1 MPa), and δ_m is in km. NSZ means no slip zone.)

Transform fault	Approximate length (km)	Total relative velocity u_0(cm/yr)	Midpoint age (Myr)	δ_T(km)	Rheology	Lithosphere thickness (km)	Depth (km) =	10	20	30
Romanche	800 Sykes (1967)	3	27	70	Dry olivine	54	T_0 =	513	730	910
							T_{max} =	1135	1135	1135
							τ =	880	600	380
							δ_m =	4.6	6.8	12
					Wet olivine	51	T_0 =	513	730	910
							T_{max} =	953	953	953
							τ =	630	351	<50
							δ_m =	5.9	11	>60
Eltanin (55° S)	850 Barazangi & Dorman (1969)	9	9	40	Dry olivine	35	T_0 =	657	980	
							T_{max} =	1185	1185	
							τ =	355	150	NSZ
							δ_m =	3.7	8.7	
					Wet olivine	34	T_0 =	657	980	
							T_{max} =	992	992	NSZ
							τ =	230	<50	
							δ_m =	5	>60	
Amsterdam (80° E, 36° S)	450 Barazangi & Dorman (1969)	7	6	33	Dry olivine	31	T_0 =	717	1086	
							T_{max} =	1173	1173	NSZ
							τ =	620	170	
							δ_m =	3.1	11	
					Wet olivine	30	T_0 =	717		
							T_{max} =	985	NSZ	NSZ
							τ =	390		
							δ_m =	5.1		

in T_0. The higher spreading rates associated with the Eltanin and Amsterdam fracture zones lead to lower shear stresses, while the relative youth of these faults tends to produce higher values of τ. However, the young ages of these faults also result in higher values of T_0, which tend to lower the shear stress. δ_m is only several kilometres at a depth of 10 km, but it increases with depth because of the increase in T_0. Although δ_m tends to decrease with the age of a fault, the higher ambient temperatures that accompany the younger ages tend to widen the shear zone. δ_T depends on age only.

The depth at which a slip zone can exist is limited by the increase of T_0 with depth. For some of the cases in Table 3, T_0 is so large that narrow slip zones cannot be maintained. The disappearance of the slip zone occurs at depths comparable to and perhaps smaller than the lithosphere thicknesses given in Table 3. The viscous part of the fault is only about twice as thick as the brittle upper portion. Thus the rate of energy dissipation, which is proportional to the product of τ with u_0 and the area of the fault, should be comparable in these different parts of the fault. Thermal anomaly thicknesses are comparable to the entire lithosphere thickness. Clearly this indicates that these viscous slip zones should be modelled three-dimensionally to account for the proximity of the surface and the asthenosphere.

6.2 BOUNDARY TRANSFORM FAULTS – THE SAN ANDREAS

Earthquakes on the San Andreas fault are not observed to occur below a depth of about 12 km (Barker 1976). Thus we have also used our model of identical half-spaces in relative motion to study the viscous slip zone that may exist at depths greater than about 12 km on this fault; Table 4 summarizes the results.

The relative motion and present age of the San Andreas were obtained from Atwater (1970). The thickness of the crust at the San Andreas fault is about 30 km (Press 1960; Kanamori & Hadley 1975). Accordingly we have modelled the viscous slip zone both in the crustal material at depths of 15 and 20 km using a wet quartzite rheology and in mantle material at a depth of 40 km using wet and dry olivine rheologies. The temperatures at these depths T_0 are from thermal models of the fault zone by Lachenbruch & Sass (1973).

If the underlying mantle has the rheology of wet olivine, a narrow viscous slip zone cannot extend more than about 10 km below the crust. However, if the mantle creeps like dry olivine, the slip zone can extend to greater depth with a larger accompanying shear stress. Brune, Henyey & Roy (1969) have shown that there would be no detectable local heat-flow

Table 4. Application of the identical half-space model to a boundary transform fault and a major continental strike–slip fault (δ_T = 42 km in all cases and NSZ means no slip zone).

	Depth (km)	Rheology	T_0(K)	T_{max}(K)	τ(bar) or (0.1 MPa)	δ_M(km)
San Andreas fault	15	Wet quartzite	625	812	225	10
(u_0 = 6 cm/yr)	20	Wet quartzite	700	812	150	18
Age ≈ 10 M yr	40	Wet olivine	950	978	<50	>20
		Dry olivine	950	1168	300	8
Central Asian strike–slip fault	50	Wet quartzite	650	767	560	12
	75	Wet olivine	750	940	715	7
(u_0 = 2 cm/yr)		Dry olivine	750	1124	1470	4
Age ≈ 10 M yr	150	Wet olivine	NSZ	NSZ	NSZ	NSZ
		Dry olivine	950	1124	840	8

anomaly along the San Andreas fault trace if the stress were 400 bar (40 MPa) or less over depths as much as 20 km. Thus, the frictional heat generated in our viscous slip-zone model could not be measured at the surface.

6.3 CENTRAL ASIAN STRIKE–SLIP FAULTS

Earthquake activity on long strike–slip faults in central Asia extends to depths of about 50 km (Chen & Molnar 1977); thus ductile behaviour must begin at a greater depth along these strike–slip faults than the ones already discussed. Table 4 gives the results of the application of our model to these continental strike–slip faults.

The relative velocity, $u_0 = 2$ cm/yr, was inferred by Chen & Molnar (1977) from the seismic moments of major earthquakes during the last century. The age of such faults is a guess based on a possible displacement of 200 km (Tapponier & Molnar 1977) having occurred at an average rate of 2 cm/yr. We computed the slip-zone structure at depths of 50, 75 and 150 km. The depth of 50 km may lie within the continental crust and accordingly we used a wet quartzite rheology; at the larger depths we employed wet and dry olivine rheologies characteristic of mantle rocks. The temperatures T_0 at these depths were taken from the continental thermal models of Froidevaux, Schubert & Yuen (1977). Shear stresses in the upper hundred kilometres are relatively large, of the order of a kilobar (100 MPa), because of the small relative velocity and low assumed temperatures.

7 Slip zones on descending slabs

At shallow depths, where the descending slab and overlying mantle are cold, their relative motion probably involves stable frictional sliding and some faulting (Stesky *et al.* 1974). The frictional heating model of Turcotte & Schubert (1973) could describe the warming of the descending slab at these shallow depths. Deeper in the mantle, the overriding plate is warmer and the oceanic crust at the top of the descending slab has also been heated by conduction from the overlying mantle and by friction. Temperatures at the top of the descending oceanic crust become sufficiently high at some depth that the relative motion is accommodated in a viscous slip zone. Only if the rocks of the oceanic crust were very resistant to deformation, as might be the case if the basalt–eclogite phase change occurs (Ahrens & Schubert 1975), would the frictional heating model of Turcotte & Schubert (1973) apply to considerable depth. At even greater depths, the overriding mantle becomes so hot that it can undergo viscous deformation; an induced secondary circulation can be established in the overriding mantle leading to a broad region of shear above the descending slab.

Because crustal rocks are weaker than mantle rocks, we will apply the model of contrasting rheologies to the viscous slip zone which occurs at intermediate depths at the top of the descending slab. Shear deformation occurs entirely within the oceanic crust. Fig. 11 shows that even after 2 Myr of subduction, the widths of shear zones are less than about 3 km compared to the average 6.5 km thickness of the oceanic crust (Shepard 1973). The variable time in the half-space model is approximately related to the distance x along the downgoing slab by $x = u_0 t$. We choose $u_0 = 10$ cm/yr.

Since the temperature near the interface of the overriding mantle and descending slab is unknown, T_0^- and T_0^+ are highly uncertain. A further complication arises since an element of oceanic crust does not experience a constant ambient mantle temperature as it descends into the mantle, whereas the model ambient mantle temperature is fixed. For reasonable choices of T_0^+, T_0^- and t, the model calculations yield a number of results which are relatively insensitive to their exact values.

We suppose that a viscous slip zone exists for distances between about 50 and 200 km along the descending slab; with $u_0 = 10$ cm/yr, t lies between about 0.5 and 2 M yr. We have chosen $T_0^+ = 400$ K, as in Figs 11–13, to characterize the low ambient temperature beneath the oceanic crust during the first few million years of subduction. The mantle just above the slip zone is considerably hotter over the distance interval 50–200 km along the slab. The temperature range, $T_0^- = 400$–1000 K used in Fig. 11 was chosen to represent these ambient mantle temperatures. If the mantle at a distance of 200 km parallel to the slab is several hundred degrees higher than 1000 K, then the notion of a narrow slip zone is no longer valid.

The case $T_0^- = 400$ K should characterize the initial stages of slip-zone development, say $t \approx 0.5$ M yr. The T_{max} values for the three crustal rheologies vary between about 620 and 960 K, while the interface temperatures are slightly lower. The maximum temperature in the crustal slip zone occurs about 1 km away from the interface; the thermal anomaly has a thickness, $\delta_T \approx 10$ km.

At larger distances along the slab, much higher values of T_0^-, similar to the values in cases (a) and (c) of Fig. 11, are appropriate. We consider cases (a) and (c) of this figure to represent the situation at $t = 2$ M yr. At this time, or at a distance of 200 km along the slab, T_{max} occurs at the interface; it varies between about 650–750 K for limestone, 850–900 K for wet quartzite and 975–1000 K for diabase even accounting for the large uncertainty in ambient mantle temperature. Between 0.5 and 2 M yr, T_{max} rises from about 600 to about 750 K for limestone, from about 800 to about 900 K for wet quartzite and from about 950 to about 1000 K for diabase; this also accounts for the large uncertainties in ambient temperature. For a given crustal rheology, the maximum temperature in the slip zone is relatively constant with distance along the slip zone and rather insensitive to temperatures in the nearby mantle and slab.

The maximum crustal temperatures given above can be used to discuss the possibility of melting on the slip zone. Since solidus temperatures are highly uncertain because of their dependence on water content (Lambert & Wyllie 1972), we will not attempt to compare them with T_{max}. The measured temperatures of lavas issuing from island arc volcanoes are probably lower bounds to the temperatures of the source magmas. These temperatures are in the range 850–1150°C (MacDonald 1972). Thus if the magmas are to originate on the slip zone, the oceanic crustal material must be heated to these temperatures. None of the crustal materials considered here are heated to 850°C after 2 M yr of subduction. The highest temperature resulting from calculations was about 750°C for diabase. Thus we must conclude that if the descending crust deforms like the materials considered here, then viscous dissipation in a slip zone is by itself inadequate to produce partial melting. The overlying mantle may be hotter than we have considered, in which case the descending oceanic crust could be further heated by conduction to the required melting temperature. In that case frictional heating contributes to the generation of magma. However, Fig. 13 shows that it plays a role of diminishing importance as the ambient mantle temperature increases.

We see no difficulty in reconciling the observation of relatively low heat flux directly behind trenches (Sugimura & Uyeda 1973; Anderson, Uyeda & Miyashiro 1976) with the occurrence of a slip zone in the descending oceanic crust and eventual partial melting therein. Although dehydration reactions can absorb a great deal of frictional heat at relatively shallow depths (Anderson *et al.* 1976), the low temperatures generated by our present models lessen the need for such a mechanism. Even should dehydration reactions in the oceanic crust be an important shallow heat sink, once these reactions have ceased to occur, the slip zone modelled here would be established on a time scale of a few tenths of a million years.

The shear stresses we have calculated for deep slip zones (several hundred bars (tens of

MPa) for diabase and wet quartzite and several bars (tenths of MPa) for limestone) are much smaller than previous estimates (Turcotte & Schubert 1973; Andrews & Sleep 1974). The weak limestone rheology may characterize the creep behaviour of the uppermost part of the descending crust where entrained sediments and water (Oxburgh & Turcotte 1976) may also contribute to the weakness of the material. If such a layer exists it serves essentially as a lubricant between the descending slab and the overriding mantle. In this case, if melting were to occur on the slip zone, it would surely be attributed to conduction from the overlying mantle.

8 Discussion; limitations of the model

Our model of viscous slip zones on descending slabs and in major transform faults is highly simplified and must be viewed only as a first step in modelling these structures. The thermal history of a material element within a slip zone can be quite complex compared with the temporal evolution assumed in the present model. Material elements in slip zones on descending slabs experience ambient mantle temperatures which change with time as the slab penetrates into the mantle. Material elements on one side of a slip zone on ridge transform faults move relative to oceanic lithosphere of varying age, temperature and thickness, on the opposite side of the fault. The situation for plate-boundary transform faults and major continental strike–slip faults is not so obvious, but ambient horizontal temperature variations parallel to the faults may certainly occur.

Our one-dimensional model accounts only for heat conduction normal to the fault plane. Heat may also flow parallel to the slip zone as is certainly the case for ridge transform faults where vertical heat conduction to the nearby surface must occur. Undoubtedly heat is also transported vertically along viscous slip zones on plate-boundary transform faults and major continental strike–slip faults, although because of their greater depths, the effect may be less important than it is for the ridge transform faults.

Gradients in the ambient mantle temperature may also influence slip-zone structure. For example, temperature variations with depth occur parallel to all the transform faults we have considered. Although a slip-zone element at a fixed depth may experience an ambient mantle temperature which is independent of time, the ambient temperature just above and below this element is different, introducing an extra dimension into the problem. We can partially account for this by applying our one-dimensional model locally, using an appropriate ambient temperature for that depth.

In addition to the above complications, which are all thermal in nature, there are numerous ways in which variations in rheological properties can influence slip-zone structure. There is always the uncertainty in extrapolating laboratory determined creep laws to predict deformation in the Earth, not to mention the difficulty in determining which rocks really control the creep behaviour of continental and oceanic crusts. Rheological parameters may vary with position along a fault. There is the obvious change from crustal to mantle creep properties that can occur on deep strike–slip continental faults; as was the case with the ambient temperature distribution, we have partly accounted for this by using the one-dimensional model locally with the appropriate rheology. Rheological properties can be different in opposite sides of a slip zone. The oceanic crust–overriding mantle contrast is a striking example, but in other cases the contrasts may not be so large as to justify confinement of all the shear to a single half-space.

Our purely viscous model does not properly describe the fault movement during the early stages of development ($t \lesssim 10^4$ yr). A one-dimensional model, similar to the one in this paper, but incorporating a visco-elastic rheology (Kanamori 1972) should be developed to

describe the early stages of fault motion. Faulting will undoubtedly occur when the shear stress is exceedingly high (above a few kilobars) at early times (Stesky *et al.* 1974; Jaeger & Cook 1976). Far from the centre of a slip zone, as the temperature becomes colder, steady-state creep may no longer describe the deformation. There, the material may become brittle and anelastic transient creep may occur (Scholz 1968; Murrell & Chakravarty 1973).

The similarity solution gives the physically implausible result that $\tau \to \infty$ as $t \to 0$. This singular behaviour is often encountered in systems whose evolution, after some initial transient, is described by similarity or boundary-layer solutions. An example is the development of the oceanic boundary layer. At the ridge, at $t = 0$, the surface heat flux is infinite according to the similarity solution. Nevertheless, similarity solutions usually give the correct physical behaviour for times not too near the origin. As an example, the decay of oceanic heat flux with the square root of age, as predicted by similarity, is known to be valid away from the ridge crest. In our problem of half-spaces in relative motion, there is no characteristic length scale other than $(kt/\rho c_p)^{1/2}$. Thus although the similarity solution may have obvious shortcomings at $t = 0$, we believe that it correctly describes the evolution of the viscous slip zone at subsequent times.

Acknowledgments

We would like to thank our colleagues at UCLA, Peter Bird, John Christie and Aaron Tovish for helpful discussions during the course of this work. Research supported by the Earth Sciences Section, National Science Foundation, under NSF grant EAR77-15198, the University of California through the Academic Senate Research Committee and the Campus Computing Network and CNEXO, France, SMC.

References

Abramowitz, M. & Stegun, I. A. (eds), 1965. *Handbook of mathematical functions*, p. 228, Dover, New York.

Ahrens, T. J. & Schubert, G., 1975. Gabbro-eclogite reaction rate and its geophysical significance, *Rev. Geophys. Space Phys.*, **13**, 383–400.

Anderson, R. N., Uyeda, S. & Miyashiro, A., 1976. Geophysical and geochemical constraints at converging plate boundaries – I. Dehydration in the downgoing slab, *Geophys. J. R. astr. Soc.*, **44**, 333–357.

Andrews, D. J. & Sleep, N. H., 1974. Numerical modelling of tectonic flow behind island arcs, *Geophys. J. R. astr. Soc.*, **44**, 237–251.

Aoki, H., 1973. Stability of transform fault as inferred from viscous flow in the upper mantle, *J. Phys. Earth*, **21**, 97–118.

Atwater, T. M., 1970. Implications of plate tectonics for the Cenozoic tectonic evolution of western North America, *Bull. geol. Soc. Am.*, **81**, 3513–3536.

Barazangi, M. & Dorman, J., 1969. World seismicity map of ESSA Coast and Geodetic Survey epicenters data for 1961 to 1967, *Bull. seism. Soc. Am.*, **59**, 369–380.

Barker, T. G., 1976. Quasi-static motions near the San Andreas fault zone, *Geophys. J. R. astr. Soc.*, **45**, 689–705.

Bird, P., Toksöz, M. N. & Sleep, N. H., 1975. Thermal and mechanical models of continent–continent convergence zones, *J. geophys. Res.*, **80**, 4405–4416.

Bird, P., 1976. Thermal and mechanical evolution of continental convergence zones: Zagros and Himalayas, *PhD thesis*, 423 pages, Massachusetts Institute of Technology, Cambridge.

Bird, P., 1978. Finite element modeling of lithosphere deformation: the Zagros collision orogeny, *Tectonophys.*, in press.

Brinkman, H. A., 1952. Heat effects in capillary flow I, *Appl. Sci. Res. A*, **2**, 120–128.

Brune, J. N., Henyey, T. L. & Roy, R. F., 1969. Heat flow, stress and rate of slip along the San Andreas Fault, California, *J. geophys. Res.*, **74**, 3821–3827.

Chen, W. P. & Molnar, P., 1977. Seismic moments of major earthquakes and the average rate of slip in central Asia, *J. geophys. Res.*, **82**, 2945–2970.

Froidevaux, C., 1973. Energy dissipation and geometric structure at spreading plate boundaries, *Earth planet. Sci. Lett.*, **20**, 419–424.

Froidevaux, C., Schubert, G. & Yuen, D. A., 1977. Thermal and mechanical structure of the upper mantle: a comparison between continental and oceanic models, *Tectonophys.*, **37**, 233–246.

Gavis, J. & Laurence, R. L., 1968. Viscous heating in plane and circular flow between moving surfaces, *Ind. Eng. Chem. Fund.*, **7**, 232–239.

Goetze, C. & Brace, W. F., 1972. Laboratory observations of high-temperature rheology of rocks, *Tectonophys.*, **13**, 583–600.

Hasebe, K., Fujii, N. & Uyeda, S., 1970. Thermal processes under island arcs, *Tectonophys.*, **10**, 335–355.

Heard, H. C., 1976. Comparison of the flow properties of rocks at crustal conditions, *Phil. Trans. R. Soc. Lond. A*, **283**, 173–186.

Herring, C., 1950. Diffusional viscosity of a polycrystalline solid, *J. appl. Phys.*, **21**, 437–445.

Jaeger, J. C. & Cook, N. G., 1976. *Fundamentals of rock mechanics*, 2nd edn, chapter 4, J. Wiley & Sons, Inc., New York.

Jischke, M., 1975. On the dynamics of descending lithospheric plates, *J. geophys. Res.*, **80**, 4809–4813.

Kanamori, H., 1972. Mechanism of tsunami earthquakes, *Phys. Earth planet Int.*, **6**, 346–359.

Kanamori, H. & Hadley, D., 1975. Crustal structure and temporal velocity change in southern California, *Pure Appl. Geophys.*, **113**, 257–280.

Kohlstedt, D. L. & Goetze, C., 1974. Low-stress high-temperature creep in olivine single crystals, *J. geophys. Res.*, **79**, 2045–2051.

Kohlstedt, D. L., Goetze, C. & Durham, W. B., 1976. Experimental deformation of single crystal olivine with application to flow in the mantle in *The physics and chemistry of minerals and rocks*, pp. 35–50, ed. Strens, R. G., J. Wiley & Sons, Inc. New York.

Lachenbruch, A. H. & Thompson, G. A., 1972. Oceanic ridges and transform faults: their intersection angles and resistance to plate motion, *Earth planet. Sci. Lett.*, **15**, 116–122.

Lachenbruch, A. H. & Sass, J. H., 1973. Thermomechanical aspects of the San Andreas fault system, pp. 192–205, *Proceedings of the conference on tectonic problems of the San Andreas fault system*, eds Kovach, R. & Nur, A., Stanford University Publication.

Lambert, I. B. & Wyllie, P. J., 1972. Melting of gabbro (quartz eclogite) with excess water to 35 kilobars, with geological applications, *J. Geol.*, **80**, 693–708.

MacDonald, G. A., 1972, *Volcanoes*, chapter 4, Prentice-Hall, Inc.

McKenzie, D. P. & Sclater, J. G., 1968. Heat flow inside the island arcs of the northwestern Pacific, *J. geophys. Res.*, **73**, 3173–3179.

Minster, J. B., Jordan, T. H., Molnar, P. H. & Haines, E., 1974. Numerical modelling of instantaneous plate tectonics, *Geophys. J. R. astr. Soc.*, **36**, 441–476.

Molnar, P. H. & Tapponier, P., 1975. Cenozoic tectonics of Asia: effects of a continental collision, *Science*, **189**, 419–426.

Murrell, S. A. F. & Chakravarty, S., 1973. Some rheological experiments on igneous rocks up to 1120°C, *Geophys. J. R. astr. Soc.*, **34**, 211–250.

Oldenburg, D. W. & Brune, J. N., 1975. An explanation of ocean ridges and transform faults, *J. geophys. Res.*, **80**, 2575–2585.

Oxburgh, E. R. & Turcotte, D. L., 1970. Thermal structure of island arcs, *Bull. geol. Soc. Am.*, **81**, 1665–1688.

Oxburgh, E. R. & Turcotte, D. L., 1976. The physico-chemical behaviour of the descending lithosphere, *Tectonophys.*, **32**, 107–128.

Parmentier, E. M., 1978. A study of thermal convection in non-Newtonian fluids, *J. Fluid Mech.*, **84**, 1–13.

Parrish, D. K., Krivz, A. L. & Carter, N. L., 1976. Finite-element folds of similar geometry, *Tectonophys.*, **32**, 183–207.

Post, R. L., Jr., 1977. High temperature creep of Mt Burnett dunite, *Tectonophys.*, **42**, 75–110.

Press,. F., 1960. Crustal structure in the California–Nevada region, *J. geophys. Res.*, **65**, 1039–1051.

Reichle, M. S., 1975. A seismological study of the Gulf of California: sonobuoy and teleseismic observations and tectonic implications, *PhD thesis*, 249 pages, University of California, San Diego.

Reid, I. & MacDonald, K., 1973. Microearthquake study of the Mid-Atlantic Ridge near 37° N, using sonobuoys, *Nature*, **246**, 88–90.

Richter, F. M., 1977. On the driving mechanism of plate tectonics, *Tectonophys.*, **38**, 61–88.

Schmid, S. M., 1976. Rheological evidence for changes in the deformation mechanism of Solenhofen limestone towards low stresses, *Tectonophys.*, **31**, T21–T28.

Scholz, C. H., 1968. Mechanism of creep in brittle rock, *J. geophys. Res.*, **73**, 3295–3302.

Schubert, G., Froidevaux, C. & Yuen, D. A., 1976. Oceanic lithosphere and asthenosphere: thermal and mechanical structure, *J. geophys. Res.*, **81**, 3525–3540.

Shepard, F. P., 1973. *Submarine geology*, 3rd edn, chapter 13, Harper & Row, New York.

Stesky, R. M., Brace, W. F., Riley, D. K. & Robin, P., 1974. Friction in faulted rock at high temperature and pressure, *Tectonophys.*, **23**, 177–203.

Stocker, R. L. & Ashby, M. F., 1973. On the rheology of the upper mantle, *Rev. Geophys. Space Phys.*, **11**, 391–426.

Sugimura, A. & Uyeda, S., 1973. *Island arcs*, chapter 1, Elsevier, New York.

Sykes, L. R., 1967. Mechanisms of earthquakes and nature of faulting on the mid-oceanic ridge, *J. geophys. Res.*, **72**, 2131–2153.

Tapponier, P. & Francheteau, J., 1978. Some remarks on the mechanisms of slowly accreting plate boundaries, *J. geophys. Res.*, in press.

Tapponier, P. & Molnar, P. H., 1977. Active faulting and Cenozoic tectonics in China, *J. geophys. Res.*, **82**, 2905–2930.

Toksöz, M. N., Minear, J. W. & Julian, B., 1971. Temperature field and geophysical effects of a downgoing slab, *J. geophys. Res.*, **76**, 1113–1138.

Turcotte, D. L. & Oxburgh, E. R., 1968. A fluid theory for the deep structure of dip–slip fault zones, *Phys. Earth planet Int.*, **1**, 381–386.

Turcotte, D. L. & Schubert, G., 1973. Frictional heating of the descending lithosphere, *J. geophys. Res.*, **78**, 5876–5886.

Turian, R. M., 1969. The critical stress in frictionally heated non-Newtonian plane Couette flow, *Chem. Eng. Sci.*, **24**, 1581–1587.

Yuen, D. A. & Schubert, G., 1976. Mantle plumes: a boundary layer approach for Newtonian and non-Newtonian temperature dependent rheologies, *J. geophys. Res.*, **81**, 2499–2510.

Yuen, D. A., Tovish, A. & Schubert, G., 1978. Shear flow beneath oceanic plates: local non-similarity boundary layers for olivine rheology, *J. geophys. Res.*, in press.